J. Fluid Mech. (1977), *vol.* 79, *part* 2, *pp.* 379–389
Printed in Great Britain

Thermal convection in a Hele-Shaw cell

By BEVERLY K. HARTLINE AND C. R. B. LISTER
Geophysics Program, University of Washington, Seattle,Washington 98195

(Received 6 August 1975 and in revised form 21 August 1976)

We derive the Rayleigh number R_{HS} for thermal convection in a Hele-Shaw cell with gap width d and full width (gap plus walls) Y. For the state of marginal stability, the system of equations is found to be formally identical to that describing flow through a uniform porous medium, if $d^3/12Y$ is identified as the Hele-Shaw permeability. Thus Lapwood's (1948) thermal-instability analysis should apply, and the critical Rayleigh number should be $4\pi^2$ when the cell has impermeable isothermal boundaries.

Baker's (1966) pH-indicator method for visualizing fluid flow has been adapted for use in a Hele-Shaw cell. In addition to revealing the convection pattern clearly, this technique proves to be an especially sensitive detector of incipient flow, and a highly accurate means of verifying the onset of convection. Our experiments confirm that the critical Hele-Shaw Rayleigh number is 40 ± 2, thereby validating our theoretically derived expression for the Rayleigh number. We also measure the vertical flow velocity w_m and find that $w_m \propto (R_{HS}^2 - 40^2)^{\frac{1}{2}}$ closely fits our data for $40 < R_{HS} < 140$.

1. Introduction

Development of geothermal power resources has increased general interest in the properties of convection in porous media. The scientific importance of the field has also been enhanced by the discovery that hydrothermal circulation is the dominant heat-transfer mechanism in young oceanic crust (Lister 1972). How far hydrothermal circulation penetrates into the earth is a fundamental parameter of natural systems. Estimates of circulation depth can be made only with an understanding of the aspect ratios that convection cells will tolerate and the amount of environmental forcing needed to distort them from their natural shape. Laboratory techniques that allow the flow in the convection cells to be visualized are very important for such investigations.

One type of laboratory apparatus lends itself especially well to the study of two-dimensional convection patterns. It exploits the mathematical similarity, first noted by Hele-Shaw (1898), between slow two-dimensional flow in a uniformly porous medium and laminar flow in a narrow slot sandwiched between parallel walls. If the walls of this 'Hele-Shaw cell' are transparent, the flow pattern can be observed by using strioscopy, shadowgraphs, schlieren photography, interferometry, or the pH-indicator method we describe in this paper. The last method is an especially sensitive detector of incipient flow and a highly

accurate way of verifying the onset of convection. Results from Hele-Shaw cell experiments are of general applicability because incipient thermal instability in a porous medium is two-dimensional, and roll convection persists to a Rayleigh number nearly ten times the critical value (Straus 1974).

True porous media are inherently heterogeneous on the scale of the pores and channels. To describe local flow, details of the channel geometry, spacing, and tortuosity are needed. A better approach for dealing with macroscopic natural phenomena treats a block of porous material as a 'black box' which passes fluid in response to a pressure gradient. In low Reynolds number flow, where the pressure–flow relationship is linear, a permeability can be defined for any material that is uniformly porous on a scale substantially larger than the channel separation (Darcy 1856). The permeability is a parameter characteristic of the matrix and allows the calculation of the flow through the porous material, solid as well as pores, per unit cross-section. A Hele-Shaw cell is a fundamental element of a cracked porous medium; in any phenomenon (such as the development of salt fingers) where the presence of the walls is immaterial to the flow, the permeability can be treated as simply the permeability of the slot. In porous convection, however, thermal conduction through the whole porous medium enters into the derivation of the Rayleigh number. The walls of the Hele-Shaw cell conduct heat; therefore their presence must be taken into account in deriving the Rayleigh number of such a cell. This paper derives the correct Rayleigh number for a thin Hele-Shaw cell, and experimentally verifies that the onset of convection occurs at a Rayleigh number equal to the theoretical prediction of $4\pi^2$ (Lapwood 1948), within the small experimental error.

2. The Hele-Shaw Rayleigh number

In thermal convection experiments, the important non-dimensional parameter is the Rayleigh number, but prior workers with Hele-Shaw cells have not calculated it correctly. Here we outline a rigorous mathematical derivation of the Hele-Shaw Rayleigh number R_{HS}, and demonstrate that it plays the same role as Lapwood's (1948) porous-medium Rayleigh number R. An independent but equivalent physical argument follows the mathematical section.

Mathematical derivation

In general, the system of equations governing thermal convection has time-independent solutions near the state of marginal stability (Chandrasekhar 1961). Therefore, in our examination of the criteria for the onset of convection in a Hele-Shaw cell heated from below, we need consider only the steady-state, first-order perturbation equations.

The cell dimensions and co-ordinate system are shown in figure 1. The steady-state, average perturbation velocity of laminar fluid flow in a planar channel of width $d \ll H$, L (H = cell height, L = cell length) is

$$\mathbf{u}' = (-d^2/12\mu)(\nabla' P' - \rho_0 \alpha g \theta' \hat{\mathbf{z}}) \tag{1}$$

(see Lamb 1932, §330). Here μ is the dynamic viscosity of the fluid, ρ_0 its density

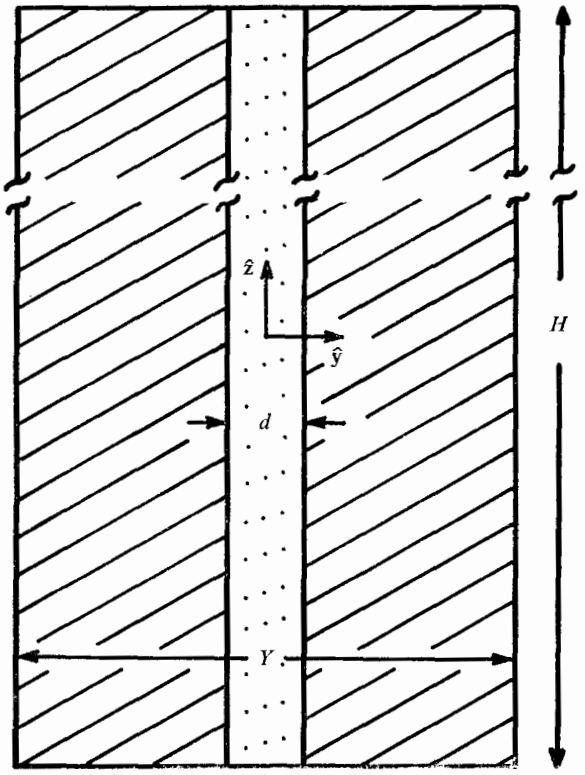

FIGURE 1. Schematic cross-section of a Hele-Shaw cell showing the dimensions and co-ordinate system referred to in the text. The hatched regions represent the cell walls, and the dotted area is fluid filled.

at a reference temperature, and α its volume thermal expansion coefficient. The perturbation pressure is P', g is the gravitational acceleration and $\hat{\mathbf{z}}$ is the vertical unit vector, positive upwards. The temperature field T' is given by

$$T' = T'_0 + \theta', \tag{2}$$

where T'_0 is the conductive temperature field, $T'_0 = (z'/H)\Delta T$, and z' is the vertical co-ordinate. The law of thermal expansion, $\rho_f = \rho_0(1-\alpha T')$, where ρ_f is the fluid density, and the Boussinesq approximation have been incorporated in the second term on the right-hand side of (1). The primes indicate dimensional quantities which will be non-dimensionalized later.

In a Hele-Shaw cell with full width (walls plus channel) $Y \ll H, L$, heat is conducted by the fluid and by the walls, but can be advected only by the fluid in the gap. Thus the steady, first-order perturbation temperature field obeys

$$\rho_f c_f d\mathbf{u}' . \nabla' T'_0 = Yk\nabla'^2\theta'. \tag{3}$$

The heat capacity of the fluid is c_f, and the thermal conductivity k is appropriate to the total system, walls plus fluid. In the sandwich geometry characteristic of a Hele-Shaw cell, when heat flows only parallel to the plane of the channel

$$k = k_f d/Y + k_w(1-d/Y), \tag{4}$$

where k_f and k_w are the thermal conductivities of the fluid and walls, respectively. To complete the mathematical description, we assume the fluid is incompressible and include the statement that matter is conserved:

$$\nabla' . \mathbf{u}' = 0. \tag{5}$$

It is instructive to write (1), (3) and (5) in dimensionless form by defining non-dimensional variables (unprimed) for length, velocity, temperature and pressure:

$$\mathbf{x} = \frac{\mathbf{x}'}{H}, \quad \mathbf{u} = \frac{Hd}{\kappa Y}\mathbf{u}', \quad T = \frac{T'}{\Delta T}, \quad P = \frac{12\kappa\nu Y}{Hd^3}P'. \tag{6a–d}$$

Here κ is a thermal diffusivity

$$\kappa = k/\rho_f c_f. \tag{7}$$

Using these, our set of equations becomes

$$\mathbf{u} = -\nabla P + R_{HS}\theta\hat{\mathbf{z}}, \tag{8}$$

$$-w = \nabla^2\theta, \quad \nabla . \mathbf{u} = 0. \tag{9), (10}$$

The vertical component of velocity is w, and ν is the kinematic viscosity of the fluid. The Hele-Shaw Rayleigh number is

$$R_{HS} = \alpha g \Delta T H d^3/12\kappa\nu Y. \tag{11}$$

For a uniform porous medium of permeability D, the analogous dimensionless equations take the form (Palm, Weber & Kvernvold 1972)

$$\mathbf{u} = -\nabla P + R\theta\hat{\mathbf{z}}, \tag{12}$$

$$-w = \nabla^2\theta, \quad \nabla . \mathbf{u} = 0, \tag{13), (14}$$

where R is Lapwood's (1948) Rayleigh number for a porous medium

$$R = \alpha g \Delta T H D/\kappa\nu. \tag{15}$$

Equations (8), (9) and (10) are formally identical to (12), (13) and (14), respectively. A comparison of (11) and (15) reveals that the Hele-Shaw Rayleigh number is identical to the porous-medium Rayleigh number if the Hele-Shaw permeability is

$$D_{HS} \equiv d^3/12Y. \tag{16}$$

By analogy, the critical Hele-Shaw Rayleigh number for a cell with impermeable isothermal boundaries should be $4\pi^2$, the value predicted by Lapwood (1948) for a uniform porous medium with the same boundary conditions.

Physical argument

The Hele-Shaw cell permeability can also be derived from a simple physical argument that compares channel flow with Darcy flow. When the two processes are described in physically synonymous terms, (16) is seen to represent the Hele-Shaw permeability.

The fluid velocity averaged over the width of a Hele-Shaw channel is

$$\mathbf{u}' = (-d^2/12\mu)(\nabla P' + \rho\mathbf{g}) = \mathbf{q}'/A_c \tag{17}$$

(Lamb 1932, §330). Here $\mathbf{q}'$ is the volume flux of fluid, $\nabla P' + \rho \mathbf{g}$ is the pressure gradient driving the flow, and A_c is the cross-sectional area of the channel. Darcy's (1856) observations of water flow through beds of sand led him to conclude that

$$\mathbf{q}'/A = (-D/\mu)(\nabla P' + \rho \mathbf{g}), \tag{18}$$

where A is the total cross-section of the porous material (solid plus pore spaces) and D is the permeability. This statement, known as Darcy's law, compares easily observable quantities (flux per unit area with pressure gradient) while combining parameters which are harder to measure or vary throughout the sample (e.g. percentage pore area in a cross-section, pore shape, channel tortuosity) in an empirical property of the porous material, known as permeability. Darcy's law operationally defines the permeability.

When the Hele-Shaw cell permeability is defined in a manner consistent with Darcy's law, then one can think of the Hele-Shaw cell as being a porous sample. The cell's walls model the solid matrix, and the gap plays the role of pore spaces. The analogy is complete for the case of thermal convection only if the temperature field is truly two-dimensional in the Hele-Shaw cell. Then the walls can be considered to be in as intimate a thermal contact with the fluid as the solid material of a finely porous matrix. This sets the requirement that the cell be 'thin' ($Y \ll H, L$), and the condition is implicit in (3). Thus

$$A_c = (d/Y)\, A. \tag{19}$$

Combining (17) and (19) and comparing with (18) allows us to identify the Darcy permeability of a Hele-Shaw cell:

$$D_{HS} = d^3/12Y. \tag{20) [or (16)]}$$

Bear (1972, p. 164) and Lister (1974) obtained an identical expression for the permeability of a horizontally infinite rock slab of thickness H whose porosity was due to parallel planar fissures of width $d \ll H$ and spacing $Y \ll H$. Physically the Hele-Shaw cell can be imagined to represent a slice of this rock: the insulated outer walls of the Hele-Shaw cell correspond to the planes of symmetry between adjacent cracks.

When the permeability of a Hele-Shaw cell is given by (20), the momentum equation for the system is identical to Darcy's law. This makes laminar flow in a Hele-Shaw cell mathematically indistinguishable from such flow in any other porous sample. Hence Lapwood's (1948) instability analysis for a Darcy material applies directly to a thin Hele-Shaw cell that meets the criterion of two-dimensionality of the temperature field. Then the Hele-Shaw Rayleigh number is $R_{HS} = \alpha g \Delta T H d^3/12\kappa\nu Y$, as was derived above.

3. Equipment and methods

We report experiments in two Hele-Shaw cells of length $L = 80$ cm and height $H = 4{\cdot}0$ cm. The cross-section of our lower porosity apparatus is shown in figure 2. Plexiglas windows 0·63 cm thick sandwich a water-filled gap. The width d of the slot is maintained by copper shims 0·10 cm thick (low porosity cell) or

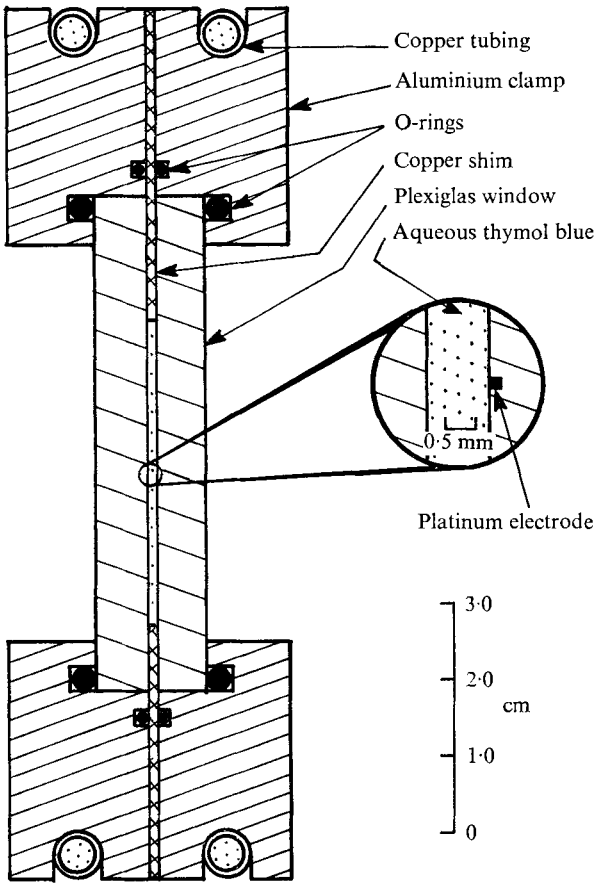

FIGURE 2. Cross-section of the lower porosity Hele-Shaw cell with a magnified view of the platinum electrode.

0·20 cm thick (high porosity cell), which also form the impermeable isothermal boundaries of the fluid-filled region. Aluminium heat sinks double as clamps to hold the assembly together. Temperature-regulated water circulates through the clamps, thereby controlling the vertical temperature difference across the cell to better than $\pm$ 0·05 °C. We record the temperature using copper–constantan thermocouples set deep in the aluminium clamps, very near the copper shims. Except when photographs are being taken, the whole apparatus is encased in ethafoam insulation 5 cm thick. To further reduce thermal interaction with the environment, the mean cell temperature is maintained near room temperature.

The temperature field must be two-dimensional for the Hele-Shaw cell to be a valid model of a uniform porous medium. This means that temperature gradients across the cell (i.e. along the y axis in figure 1) must be small compared with the gradients in the plane of the cell. Since the walls of our Hele-Shaw cells are relatively thick, we were concerned about meeting this criterion. Preliminary qualitative results have been obtained from a cell 80 cm long and 4·0 cm tall, with a gap width of about 0·1 cm but with walls only 0·08 cm thick. The convection

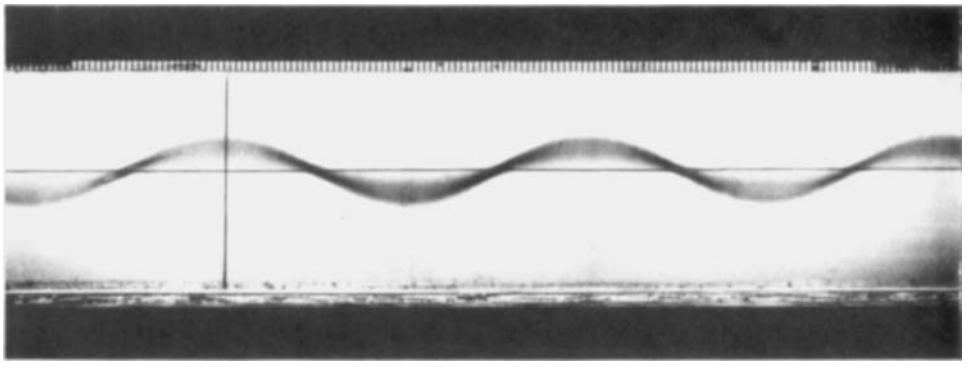

FIGURE 3. Photograph of the dye line, 40 s after initiation, in our lower porosity Hele-Shaw cell at $R_{HS} = 47$ ($\Delta T = 3{\cdot}7\,^{\circ}\mathrm{C}$, mean temperature of $21{\cdot}2\,^{\circ}\mathrm{C}$). The view is of the central 16 cm in an apparatus which is 80 cm long. The scale along the top edge is in millimetres, and the vertical line is a reference line.

pattern is indistinguishable from that in the thicker cell: at low Rayleigh numbers the midline vertical velocity profile is essentially sinusoidal with a wavelength of $1{\cdot}6 \pm 0{\cdot}2$ times the fluid depth. As the Rayleigh number exceeds about 120 the circulation pattern gradually develops features of boundary-layer flow. The cores of the convection half-cells are relatively stagnant, while comparatively narrow upwelling and descending 'plumes' define the perimeters. The structure, scale and evolution of the patterns are identical for the thin- and thick-walled Hele-Shaw cells, so that the validity of results from the thick-walled cells is confirmed.

We have adapted Baker's (1966) pH-indicator technique of flow visualization for use in a Hele-Shaw cell. A platinum wire of small diameter (0·012 cm) is embedded in one of the Plexiglas walls of our cell (figure 2). This ensures that the wire is in contact with the fluid without interfering with the Poiseuille (channel) flow. A voltage pulse (18 V d.c.) a few seconds long is imposed between this electrode and the metallic top and bottom boundaries of the fluid-filled region. The electron transfer reaction changes the local pH, thereby changing the colour of the aqueous thymol blue solution near the wire. This coloured band serves as a Lagrangian marker, and reveals the mid-cell flow pattern (figure 3, plate 1). Eventually the coloured band disappears.

The time-dependent displacement of the dye line from the platinum wire is a measure of fluid velocity. Incipient flow ($< 10^{-4}$ cm/s) can be detected readily; this corresponds to a Nusselt number of less than 1·01. To facilitate comparison of the velocities observed in the two different cells, the velocity has been non-dimensionalized by multiplying by $Hd/\kappa Y$. This form of the velocity scale was justified in the formal theoretical section.

Although Baker's (1966) flow-visualization technique reveals the convection pattern well, there are significant difficulties in obtaining accurate velocity measurements in our cell. Since the platinum wire electrode is embedded in one of the Plexiglas walls (figure 2), we rely on diffusion to spread the coloured band across the width of the cell. When the platinum electrode is the anode, it creates an acidic line; when it is the cathode, a basic line is produced. The dominant chemical species of interest are therefore hydronium ions and hydroxyl ions; their respective diffusion constants in aqueous solution at 20 °C are $8{\cdot}5 \times 10^{-5}$ cm^2/s† and about 5×10^{-5} cm^2/s (Harned & Owen 1950, p. 172). Monte-Carlo computer simulation of diffusion into a Poiseuille flow profile has shown that the mean velocity of the dye line approaches the mean fluid velocity after 4–7 s of dye-line existence. The shorter time applies to H_3O^+ diffusion and the longer time to OH^- diffusion. The velocities we report were all measured over a time interval which began more than 12 s after the dye line was initiated. Therefore, the velocity is not measured at $z' = \frac{1}{2}H$, but rather at a distance from this midline which increases with the flow velocity. We have corrected the raw velocity data to a midline velocity w_m by assuming that the vertical velocity w varies with z' according to the relation

$$w(z') = w_m \sin(\pi z'/H). \tag{21}$$

† *American Institute of Physics Handbook*, 3rd edn, pp. 2–226. McGraw-Hill, 1972.

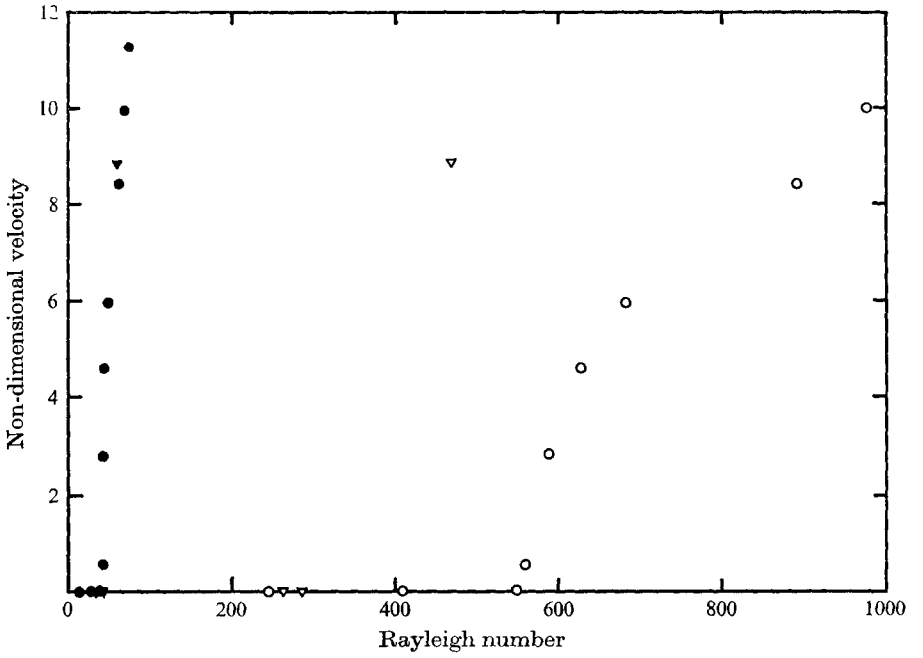

FIGURE 4. Linear plot of velocity against Rayleigh number. The fluid velocity has been non-dimensionalized by multiplying by $Hd/\kappa Y$. Solid symbols, Rayleigh number calculated from (11); open symbols, Rayleigh number calculated from (23). ●, ○, from experimental apparatus (figure 2) with $d = 0{\cdot}10$ cm and $Y = 1{\cdot}37$ cm; ▼, ▽, from Hele-Shaw cell with $d = 0{\cdot}20$ cm and $Y = 1{\cdot}47$ cm.

This is consistent with the relevant differential equations when w is small, and probably remains representative of the vertical velocity distribution until boundary-layer flow is well established.

4. Experimental verification of expression for Rayleigh number

To test the validity of (11) and (16) we have compared the Rayleigh number at which instability first occurs with Lapwood's (1948) prediction of $4\pi^2$. In figure 4, the non-dimensional fluid velocity is plotted against Rayleigh number. This provides a graphic demonstration of the dramatic onset of convection.

The Rayleigh numbers for the solid symbols were calculated from (11). These data indicate a critical Rayleigh number of 40 ± 2, in excellent agreement with Lapwood's (1948) theory. The triangles and circles (data from Hele-Shaw cells with porosities of 0·136 and 0·073, respectively) lie on the same curve, which is what one would expect if the Nusselt number were a unique function of Rayleigh number and independent of the porosity.

The open symbols incorporate the same velocity measurements, but the traditionally accepted expression for Hele-Shaw cell permeability (Elder 1965; Bories 1970; Horne & O'Sullivan 1974; Williams *et al.* 1974),

$$D_{HS}^{+} = \tfrac{1}{12} d^2, \tag{22}$$

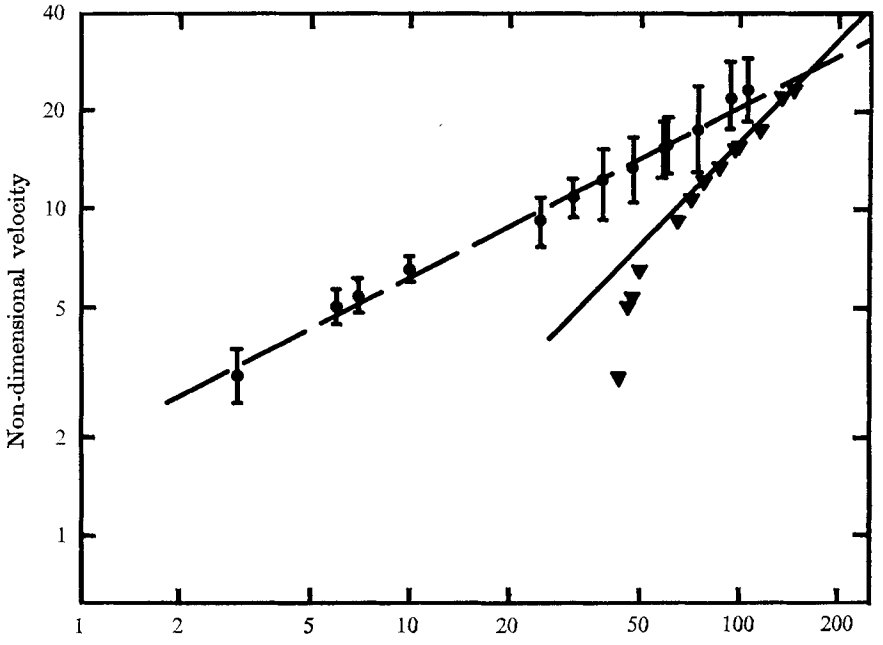

FIGURE 5. Logarithmic graph based on a Rayleigh number calculated from (11) for the complete experimental range of the Hele-Shaw cell with $d = 0{\cdot}10$ cm and $Y = 1{\cdot}37$ cm.

Circles. Plot of non-dimensional velocity against supercritical Rayleigh number ($R_{HS} - 40$). The least-squares line has a slope of 0·53. The error we associate with each velocity point represents the worst possible error in measuring the displacement, divided by the time interval during which the measurement was made. As the fluid velocity increases, the measurement time interval decreases, so the error increases with Rayleigh number.

Triangles. Plot of non-dimensional velocity against Rayleigh number. The least-squares line through the last seven points has a slope of 1·06. The error bars indicated for the circles apply to the corresponding triangles.

is used to calculate the Rayleigh number:

$$R^{+}_{HS} = \alpha g \Delta T H d^2 / 12 \kappa \nu. \tag{23}$$

Data for the two porosities indicate different critical Rayleigh numbers (about 300 and 500), neither of which agrees at all with Lapwood's (1948) predicted value. Therefore (23) cannot be the correct formula for the Hele-Shaw Rayleigh number and (22) does not represent the Darcy permeability of a Hele-Shaw cell.

5. Discussion

Numerical and experimental studies of heat transfer in porous media have diverse findings. Elder (1967) obtained experimental results which indicate that the Nusselt number N increases linearly with the Rayleigh number. Asiz & Combarnous (1970) report the results of a numerical calculation which suggests that $N \propto R^{\frac{1}{2}}$.

The convective heat transfer depends on the fluid velocity, the temperature distribution in the fluid, and the geometry of the convection cells. Without thoroughly surveying these three aspects of the flow, we can only speculate about the implications of our velocity measurements for the Nusselt number.

As the flow velocity increases, the time it takes a packet of fluid to complete a circuit of a half-cell decreases. The fluid spends less time being heated and cooled near the bottom and top boundaries, so the heat transfer into the fluid should become less efficient. Therefore, in order for the Nusselt number to be proportional to the Rayleigh number, the flow velocity must increase faster than linearly with Rayleigh number.

Figure 5 suggests that, although the velocity does not increase linearly with Rayleigh number at low Rayleigh numbers, it may approach linearity at higher Rayleigh numbers. This may be in substantial agreement with Elder (1967). Figure 5 also shows that in the range studied the data are compatible with

$$w_m \propto (R-40)^{\frac{1}{2}}, \tag{24}$$

although there is no good physical reason for such a dependence. Hence it is worthwhile to note that a better fit to our data is obtained with

$$w_m \propto (R^2-40^2)^{\frac{1}{2}}. \tag{25}$$

This is a hyperbola which behaves as $(R-40)^{\frac{1}{2}}$ at low Rayleigh numbers, but which approaches being linear with R at higher Rayleigh numbers.

6. Conclusions

Recent workers using Hele-Shaw cells to model thermal convection in a porous slab have mistakenly adopted $\frac{1}{12}d^2$ as the permeability (Elder 1965; Bories 1970; Williams *et al.* 1974; Horne & O'Sullivan 1974). The error introduced by basing the Rayleigh number on this permeability is a factor equal to the reciprocal of the porosity. Since commonly used Hele-Shaw cells have porosities of about 0·3, the calculated Rayleigh number is too large by only a factor of around 3. This is not particularly serious when the cells are used primarily to visualize flow patterns, as these change only weakly with Rayleigh number.

By properly identifying the Hele-Shaw permeability as $d^3/12Y$ we have demonstrated that the Hele-Shaw cell can be a powerful tool for quantitative study of two-dimensional flow in porous media. Not only can the convection pattern be observed, but precise velocity measurements are feasible using Baker's (1966) pH-indicator method. Infrared photography, schlieren photography or interferometry allows visualization of the temperature distribution. Direct temperature measurements can be made by sensors on the outside of the cell walls without interfering with the flow. All results can be correlated accurately with the Rayleigh number, so meaningful generalizations about thermal convection in porous samples can be made.

This work was supported by the National Science Foundation under Grant DES 74-22160. During the initial phases of the study, B.K.H. was the recipient

of a National Science Foundation Traineeship administered by the University of Washington. We thank Dr John R. Booker for helpful discussions and advice during the preparation of this manuscript. Fred Hartline aided in computer programming the dye-line diffusion problem. We are indebted to Professor G. K. Batchelor for suggesting improvements to our theoretical argument.

REFERENCES

ASIZ, K. & COMBARNOUS, M. 1970 Transfert de chaleur par convection naturelle dans une couche poreuse horizontale. *C. R. Acad. Sci., Paris*, **271**, 813–815.

BAKER, D. J. 1966 A technique for the precise measurement of small fluid velocities. *J. Fluid Mech.* **26**, 573–575.

BEAR, J. 1972 *Dynamics of Fluid in a Porous Medium*. Elsevier.

BORIES, S. 1970 Sur les mécanismes fondamentaux de la convection naturelle en milieu poreux. *Rev. Gén. Therm.* **108**, 1377–1401.

CHANDRASEKHAR, S. 1961 *Hydrodynamic and Hydromagnetic Stability*, chap. 1. Oxford: Clarendon Press.

DARCY, H. 1856 *Les Fontaines Publiques de la Ville de Dijon*. Paris.

ELDER, J. W. 1965 Physical processes in geothermal areas. *Am. Geophys. Un. Mon.* **8**, 211–239.

ELDER, J. W. 1967 Steady free convection in a porous medium heated from below. *J. Fluid Mech.* **27**, 29–48.

HARNED, H. S. & OWEN, B. B. 1950 *The Physical Chemistry of Electrolytic Solutions*. Reinhold.

HELE-SHAW, H. S. J. 1898 *Trans. Inst. Naval Archit.* **40**, 21.

HORNE, R. N. & O'SULLIVAN, M. J. 1974 Oscillatory convection in a porous medium heated from below. *J. Fluid Mech.* **66**, 339–352.

LAMB, H. 1932 *Hydrodynamics*, 6th edn. Cambridge University Press.

LAPWOOD, E. R. 1948 Convection of a fluid in a porous medium. *Proc. Camb. Phil. Soc.* **44**, 508–521.

LISTER, C. R. B. 1972 On the thermal balance of a mid-ocean ridge. *Geophys. J. Roy. Astr. Soc.* **26**, 515–535.

LISTER, C. R. B. 1974 On the penetration of water into hot rock. *Geophys. J. Roy. Astr. Soc.* **39**, 465–509.

PALM, E., WEBER, J. E. & KVERNVOLD, O. 1972 On steady convection in a porous medium. *J. Fluid Mech.* **54**, 153–161.

STRAUS, J. M. 1974 Large amplitude convection in porous media. *J. Fluid Mech.* **64**, 51–63.

WILLIAMS, D. L., VON HERZEN, R. P., SCLATER, J. G. & ANDERSON, R. N. 1974 The Galapagos spreading centre: lithospheric cooling and hydrothermal circulation. *Geophys. J. Roy. Astr. Soc.* **38**, 587–608.